FORM TI-12
8/94

CONF-960420--5
WAPD-T-3083
CONF-960588--1

Strain Energy Density-Distance Criterion for the Initiation of Stress Corrosion Cracking of Alloy X-750

M. M. Hall, Jr.
D. M. Symons

DE-AC11-93PN38195

BETTIS ATOMIC POWER LABORATORY WEST MIFFLIN, PENNSYLVANIA 15122-0079

Operated for the U.S. Department of Energy
by WESTINGHOUSE ELECTRIC CORPORATION

Meryl M. Hall, Jr.[1] and Douglas M. Symons[1]

STRAIN ENERGY DENSITY - DISTANCE CRITERION FOR THE INITIATION OF STRESS CORROSION CRACKING OF ALLOY X-750

REFERENCE: Hall, M. M., Jr., Symons, D. M., "Strain Energy Density - Distance Criterion for the Initiation of Stress Corrosion Cracking of Alloy X-750, "Effects of Environment on the Initiation of Crack Growth," ASTM STP 1298, W. A. Van Der Sluys, R. S. Piasicik, and R. Zawierucha, Eds., American Society for Testing and Materials, 1997.

ABSTRACT: A strain energy density-distance criterion[2] was previously developed and used to correlate rising-load K_C initiation data for notched and fatigue precracked specimens of hydrogen precharged Alloy X-750. This criterion, which was developed for hydrogen embrittlement (HE) cracking, is used here to correlate static-load stress corrosion cracking (SCC) initiation times obtained for smooth geometry, notched and fatigue precracked specimens. The onset of SCC crack growth is hypothesized to occur when a critical strain, which is due to environment-enhanced creep, is attained within the specimen interior. For notched and precracked specimens, initiation is shown by analysis to occur at a variable distance from notch and crack tips. The initiation site varies from very near the crack tip, for highly loaded sharp cracks, to a site that is one grain diameter from the notch, for lower loaded, blunt notches. The existence of hydrogen gradients, which are due to strain-induced hydrogen trapping in the strain fields of notch and crack tips, is argued to be controlling the site for initiation of cracking. By considering the sources of the hydrogen, these observations are shown to be consistent with those from the previous HE study, in which the characteristic distance for crack initiation was found to be one grain diameter from the notch tip, independent of notch radius, applied stress intensity factor and hydrogen level.

KEYWORDS: SCC initiation, notches, cracks, smooth surfaces, strain energy criterion, hydrogen

---

[1] Manager and Senior Engineer, respectively, Bettis Atomic Power Laboratory, Westinghouse Electric Corporation, PO Box 79, West Mifflin, PA 15122

[2] M. M. Hall, Jr., D. M. Symons and J. J. Kearns, in The Parkins Symposium on Fundamental Aspects of Stress Corrosion Cracking, The Minerals, Metals & Materials Society, 1992.

Designers of nuclear reactors must consider the potential for stress corrosion cracking (SCC) failures of reactor components that have sharp, crack-like manufacturing defects. Fatigue precracked fracture mechanics test specimens are commonly tested to determine the threshold stress intensity factors, elapsed times and crack growth rates for the onset and propagation of SCC in these defected components. Notched and smooth geometry specimens also must be tested as SCC failures have been reported for highly loaded components, such as age-hardened NiCrFe Alloy X-750 fasteners and pins, even though they were nominally free of manufacturing defects [1-3].

The stress parameter that is used to correlate SCC initiation data is chosen to suit the test specimen geometry. The fracture mechanics stress intensity factor, K, is available to correlate times for the onset of SCC crack growth for precracked specimens. A quantity $K/\sqrt{\rho}$, which is a ratio of the stress intensity factor and the square root of the notch root radius, has been used to correlate SCC initiation times for notched specimens [4]. The applied tensile stress is commonly used for uniaxial tension and bend specimens. A purpose of the work reported here is to develop a fracture mechanics stress parameter that is capable of correlating the stress conditions for initiation of SCC crack growth in smooth, notched and precracked geometry test specimens. A further purpose is to use test results obtained from these specimen types to infer aspects of the mechanisms for initiation of SCC crack growth in Alloy X-750.

PREVIOUS WORK - HYDROGEN EMBRITTLEMENT

A criterion for the initiation of intergranular cracking due to hydrogen embrittlement of Alloy X-750 was developed and reported by the authors in a previous publication [5]. As-notched and fatigue precracked three-point bend specimens were hydrogen precharged and tested in air at 93°C under rising load to determine the critical applied stress intensity factors, $K_{\rho c}$ and K_c, respectively, for the onset of cracking. Analysis of these data, using an elastic-plastic analysis of the strain energy density distributions about a notch, showed that the critical condition for the onset of crack growth is the attainment of a critical strain energy density (SEDEN), W_c, at a microstructurally characteristic distance, X_c, from the notch and fatigue crack tips. This characteristic distance was found by analysis of the data to be one grain diameter, independent of stress intensity factor, notch radius, and hydrogen concentration. This result was obtained for two heat treatment conditions of Alloy X-750, HTH and AH, having grain diameters of about 125 μm and 20 μm, respectively.

There is additional information from the hydrogen embrittlement cracking study that supports the existence of a characteristic distance for crack initiation. Fig. 1 is a photomicrograph, obtained since first publication of the HE analysis results, that shows a detached grain boundary microcrack located one grain diameter below the notch of an HTH specimen. The rising load test of this specimen was interrupted just prior to $K_{\rho c}$ and the onset of crack growth. This micrograph supports the analysis result that crack initiation occurs within the specimen interior and that the characteristic distance is one grain diameter.

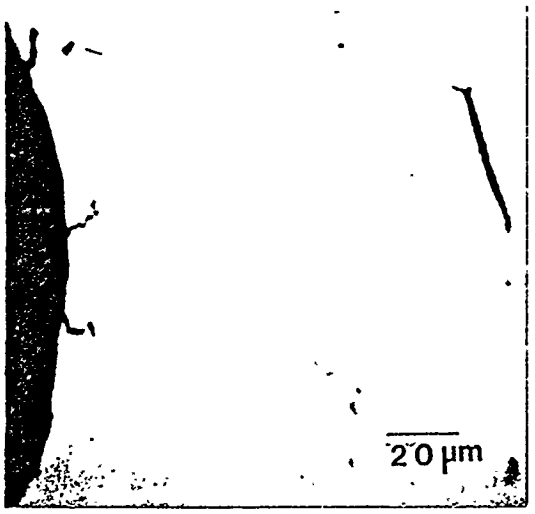

Fig. 1--Initiation of a grain boundary crack at a distance on one grain diameter below the notch tip.

The critical stress intensity factor, $K_{\rho c}$, for initiation of HE crack growth in as-notched specimens was successfully modelled as

$$K_{\rho c} = \sqrt{\frac{2}{C_p}\left(1+\frac{(1-\nu)}{4}\frac{\rho}{X_c}\right)}\sqrt{\frac{\pi E' W_c X_c}{(1-\nu)}} . \qquad (1)$$

The critical stress intensity factor increases in direct proportion to the square root of the notch root radius, ρ, for notch root radii that are large compared to the characteristic distance, X_c. As the notch root radius decreases to zero, the plastic correction factor, C_p, approaches a value of 2, and $K_{\rho c}$ approaches the critical stress intensity factor for a crack, K_c, where

$$K_c = \sqrt{\frac{\pi E' W_c X_c}{(1-\nu)}} . \qquad (2)$$

In these equations $E' = E/(1-\nu^2)$ where E and ν are the usual elastic constants. Eq. 1 defines a notch similarity function, F_ρ, such that

$$F_\rho = \sqrt{\frac{2}{C_p}\left(1+\frac{(1-\nu)}{4}\frac{\rho}{X_c}\right)} . \qquad (3)$$

Then Eq. 1 becomes

$$K_{\rho c} = F_\rho K_c . \qquad (4)$$

APPLICATION TO SCC INITIATION

Eq. 4 was developed for the time-independent rising load HE tests. We assume that this similarity relationship between notches and sharp cracks holds at all times for the time-dependent SCC test. This means that for any given notch, having a radius ρ and an applied stress intensity factor K_ρ, there is an equivalent crack, having an applied stress intensity factor, K_c, that initiates SCC at the same time, t_i, as the notch. (Note that K_ρ is calculated using stress intensity factor equations for cracks and assuming a crack length that is equal to the depth of the notch being analyzed.) Then K_c is the effective notch stress intensity factor. To obtain an expression for K_c in terms of the applied notch stress intensity factor, K_ρ, we rearrange Eq. 4, let $K_c = K_c$ and $K_{\rho c} = K_\rho$, and obtain

$$K_c = K_\rho / F_\rho. \tag{5}$$

This relationship is illustrated in Fig. 2.

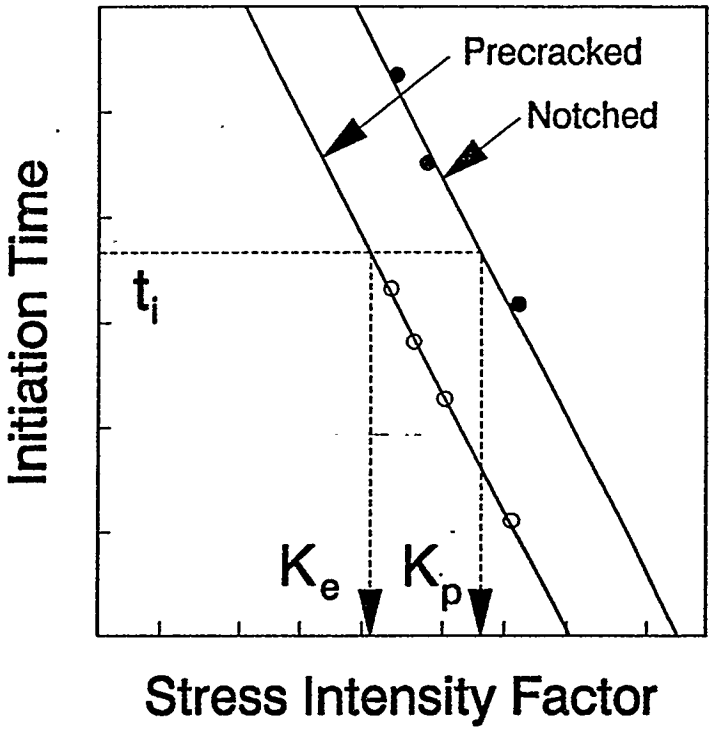

Fig. 2--Schematic illustration of the effective notch stress intensity factor concept.

Once K_c has been determined by combining notched with precracked data and using the method illustrated in Fig. 2, the characteristic distance can be obtained by

combining Eq. 3 with Eq. 5 and solving:

$$X_c = \frac{(1-\nu)\frac{\rho}{4}}{\frac{C_p}{2}\left(\frac{K_\rho}{K_e}\right)^2 - 1}. \tag{6}$$

Using the strain energy density equations previously developed, [5], we can now calculate the strain energy density at this characteristic distance :

$$W_\rho(x_c) = \frac{1-\nu}{\pi}\frac{C_p K_\rho^2}{E'\left(x_c + \frac{1-\nu}{4}\rho\right)}. \tag{7}$$

This equation also applies to cracks when $\rho = 0$. When the notch radius is large relative to X_c , the strain energy density is given by

$$W_\rho = \frac{4}{\pi}\frac{C_p K_\rho^2}{E'\rho}. \tag{8}$$

This equation establishes the relationship between the strain energy density, used in this work, and the ratio $K_\rho/\sqrt{\rho}$, which has been used by others [4] to correlate notch fracture toughness and SCC initiation data.

For smooth geometry uniaxial test specimens, the strain energy is uniformly distributed across the test section so that strain energy density is no longer dependent on position within the gage section. In this case,

$$W = \frac{1}{2}\frac{\sigma_o^2}{E} + \int_{\varepsilon_o}^{\varepsilon}\sigma d\varepsilon, \tag{9}$$

where σ_o and ε_o respectively are the yield stress and yield strain at the proportional limit. The first term on the right hand side of equation is the yield strain energy density, W_o , and the second term is an elastic-plastic (post-yield) component. Eq. 7 and Eq. 9 are used below for correlating the stress conditions for initiation of SCC crack growth in as-notched, precracked and smooth geometry test specimens. Use of Eq. 6 to determine the characteristic distance for SCC and comparison to the characteristic distances previously found for HE cracking provides further insight into the micromechanics and mechanisms for deaerated water SCC initiation in Alloy X-750.

MATERIALS AND EXPERIMENTAL PROCEDURE

Three heats of material were tested. The ranges of chemical composition are given in Table 1. Heat 1 was given the HTH heat treatment, which consists of a solution anneal at 1094°C for 1 hour, air cool and age at 704°C for 20 hours. Heats 2 and 3 were given the AH heat treatment, which consists of a stress equalization heat treatment at 885°C for 24 hours, air cool and age at 704°C for 20 hours. Table 2 provides the mechanical properties.

Table 1--Materials Compositions [wt. %]

Ni	Cr	Nb + Ta	Ti	Al	Fe	C	S
70.7-73.6	14.9-15.4	0.96-1.05	2.37-2.58	0.75-0.78	6.45-7.90	0.03-0.04	0.01 HT 1&2 0.07 HT 3

Table 2--Mechanical Properties

Heat	Test Direction	K_{JC} MPa $\sqrt{m}$	UTS MPa	Yield Strength MPa	Prop. Limit MPa	Elongation %	RA %	Gage Dia. mm	Gage Length mm
HT 1	Long.	147	1186	775	414	28	36	12.88	50.8
HT 2	Long.	150	1150	710	552	29	---	12.85	50.8
HT 3	Long.	150	1186	752	552	24	34	12.83	50.8

Microstructural features relevant to this study include grain size and grain boundary carbide size and spacing. Both the HTH and the AH heat treatments result in equiaxed grain microstructures with the mean intercept grain sizes being 127 μm for HTH and 19 μm for AH. The predominate intergranular precipitate for condition HTH is closely spaced (about 90% grain boundary coverage) $M_{23}C_6$ carbides having a range of size typically 0.1 μm to 0.3 μm. The predominate intergranular precipitate for condition AH is less closely spaced (less than about 60% grain boundary coverage) MC carbides having a size typically less than or equal to approximately 0.1 μm.

The superior SCC resistance of the HTH material in water precludes obtaining SCC initiation on smooth tensile specimens for sensible loads and reasonable times. Tests of the HTH material were performed, therefore, on as-notched and precracked compact tension specimens having a width of 20.3 mm and a thickness of 10.2 mm. The notch and crack depth to specimen width ratios were nominally 0.5. The notch root radii were 0.127 mm, 0.254 mm and 0.756 mm. Precracked specimens loaded to 33 MPa$\sqrt{m}$ were precracked with a final maximum K_I of 20 MPa$\sqrt{m}$ and those loaded

to below 33 MPa$\sqrt{m}$ were precracked with a maximum K_I of 11 MPa$\sqrt{m}$. All specimens were bolt loaded using a load transfer technique. The specimen was loaded to 95% of the final load in a tensile machine, then the load was transferred to the specimen while maintaining the CMOD constant [6]. The load transfer technique was used in reverse to measure the remaining load on the specimen at specific intervals, thereby allowing the internal crack length to be calculated by standard compliance techniques [7]. SCC incubation was measured as the time to grow an average crack of 125 μm measured. The SCC initiation time for the notched specimens was taken as the time when a crack could be detected using a stereo microscope by viewing the notch tip along the thickness. Once initiation was observed, the specimen was inserted into the autoclave for one additional cycle. In every case, the additional cycle resulted in extensive crack growth.

Testing of the AH material Heat 3 was performed using the bolt-loaded as-notched compact tension specimens and test methods discussed above. Testing of Heat 2 was performed using constant load round tensile specimens. Tensile specimens included smooth, circumferentially notched and single edge notched (saw cut) fatigue precracked specimens. Testing of notched and precracked rounds was conducted in order to facilitate comparisons to results obtained on the smooth surface uniaxial tension specimens. Testing under constant load facilitated detection of SCC initiation for the very long lived uniaxial smooth and circumferentially notched tensile specimens. In this case, SCC initiation time was taken as the specimen failure time corrected for crack growth. The maximum correction was about 19% for the shortest lived notched specimen. The smooth tensile specimens had a diameter of 10.6 mm. The as-notched tensile specimens had a major diameter of 10.6 mm and a minor diameter of 6.4 mm. The precracked tensile specimens had a diameter of 4.57 mm with a saw cut edge notch 0.30 mm deep. The onset of crack growth and the crack growth rate in the precracked specimens were determined by interim examinations to detect crack extension at the specimen surface.

The intergranular fracture surfaces for HE and SCC have the appearance of an intergranular microvoid initiation process initiating at the grain boundary carbides followed by void growth and coalescence [8]. The effect of internal hydrogen (HE tests) is to reduce the apparent level of strain associated with microvoid growth. The SCC fracture surfaces have the appearance of less void growth than the HE fracture surfaces.

All specimens were tested in an autoclave at 360°C. The water chemistry contained 40-60 STP cc H_2/kg H_2O. The room temperature pH was controlled between 10.1 and 10.3 with the oxygen less than 100 ppb, normally below 40 ppb, and the conductivity was below 80 μS/cm.

ANALYSIS PROCEDURE AND RESULTS

Fig. 3 shows the SCC initiation times that were obtained on both the Condition AH and HTH heats plotted versus strain energy density. The data reduction began with the smooth tensile specimens of AH Heat 2. Since for tensile specimens the strain energy is not dependent on position within the gage section, these data can be analyzed independent of a knowledge of the characteristic distance. Eq. 8 was used

to calculate the applied strain energy densities for the tensile specimens. In order to obtain the best fit and to account for the survival of the longest exposed specimens, a threshold strain energy value, W_{th}, having a magnitude of about 0.86 MN-m/m^3 had to be subtracted from the calculated value of the applied strain energy for each. The magnitude of W_{th} is about 7 % greater than the strain energy required for yielding (at the proportional limit), W_o. This result implies that plastic strain is a necessary condition for SCC initiation for this material. The threshold tensile stress W_{th} is about 572 MPa.

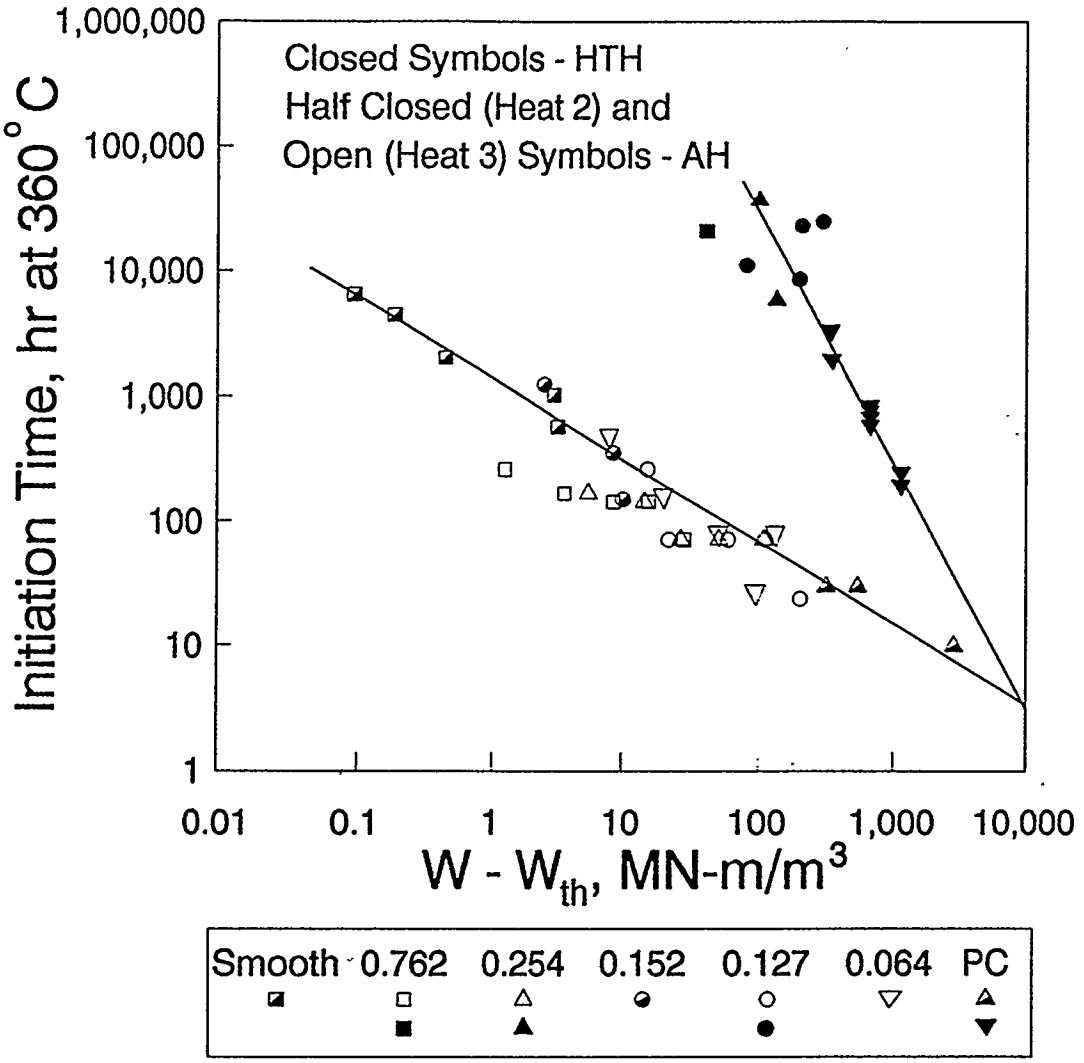

Fig. 3--SCC initiation time as a function of the applied strain energy density. Smooth, notched and precracked specimen data are correlated with a single stress parameter.

Next, using Eq. 7, the applied strain energy densities for the precracked tensile specimens were determined. A value for the sum $r_c = X_c + (1-\nu)\rho/4$ found in the denominator of Eq. 7 was adjusted so as to obtain the best fit with the smooth tensile test results. A value for r_c of about 2.5 μm was obtained. Note that this is significantly smaller than the comparable value found for the condition AH material in

the HE studies. In the HE studies X_c was found to be equal to the grain size of about 20 μm and the effective crack tip radius for precracked specimens was found to be about 8.9 μm, which gives a value for r_c of about 21.9 μm. If we assume that the effective crack tip radius in the SCC tests is 8.9 μm as found for the HE tests, we find that X_c for the precracked SCC specimens is about 0.1 μm. As is discussed in more detail below, X_c for SCC is found by analysis of the SCC data to be variable, having a range of values, from a minimum of about 0.1 μm for highly loaded cracks to a value approximately equal to the grain size for lower loaded blunt notches.

No tensile SCC initiation tests were conducted for the more SCC resistant condition HTH heat. Subsequently, there are no tensile SCC data for use in establishing r_c for precracked specimens. Therefore, strain energy density values were calculated for the precracked HTH specimens assuming the value of r_c found for the precracked AH specimens. In this way the upper curve in Fig. 3 was constructed. Note that with this assumption, the HTH and AH curves intersect at a time of about 3 hours and a SEDEN value of about 10,000 MN-m/m^3. Using this SEDEN value and Eq. 2, a K_c of about 153 MPa $\sqrt{m}$ is calculated. This is within 4% of the inert environment K_{JC} fracture toughness for both heat treatment conditions of Alloy X-750. These results indicate very short times for SCC initiation for applied stress intensity factors approaching K_{JC} and imply that the toughness is little effected by the environment during these short times.

The characteristic distances were determined next for the as-notched CT specimens of both the AH and the HTH heats using Eq. 6. The $K_{\rho e}$ values were determined in a manner consistent with the method illustrated in Fig. 2. With X_c for each specimen determined, Eq. 7 was used to plot the position of each notched specimen on Fig. 3. Note that the AH Heat 3 data fall below the best fit curve obtained for Heat 2 by about 30%. This difference is well within the normal heat-to-heat variability observed for this heat treatment of Alloy X-750.

Fig. 4 is a plot of the X_c values plotted versus a normalized applied strain energy density, $W_N = (W-W_{th})/(W_{JC}-W_{th})$. W_{JC} is the SEDEN value corresponding to K_{JC}. This figure shows that, for the AH heats, X_c increases as W decreases, with X_c approaching a value approximately equal to the AH grain size as W approaches the threshold value, W_{th}. For the HTH heat, there are no data at the lower W values from which to judge data trends near threshold. However, for both AH and HTH heats, X_c decreases as W increases.

As shown by the data trend curves in this figure, both the AH and HTH data sets are consistent with X_c approaching the grain size as W_N approaches 0 and a value of about 0.1 μm when W_N approaches 1. A value of 0.1 μm is within a factor of 2-3 the size and spacing of grain boundary carbides. Recalling the relationship, Eq. 8, between SEDEN and the ratio $K_\rho/\sqrt{\rho}$, Fig. 4 shows that X_c decreases with either a decrease in ρ or an increase in the applied K. Increases in ρ and decreases in K both lead to increases in X_c.

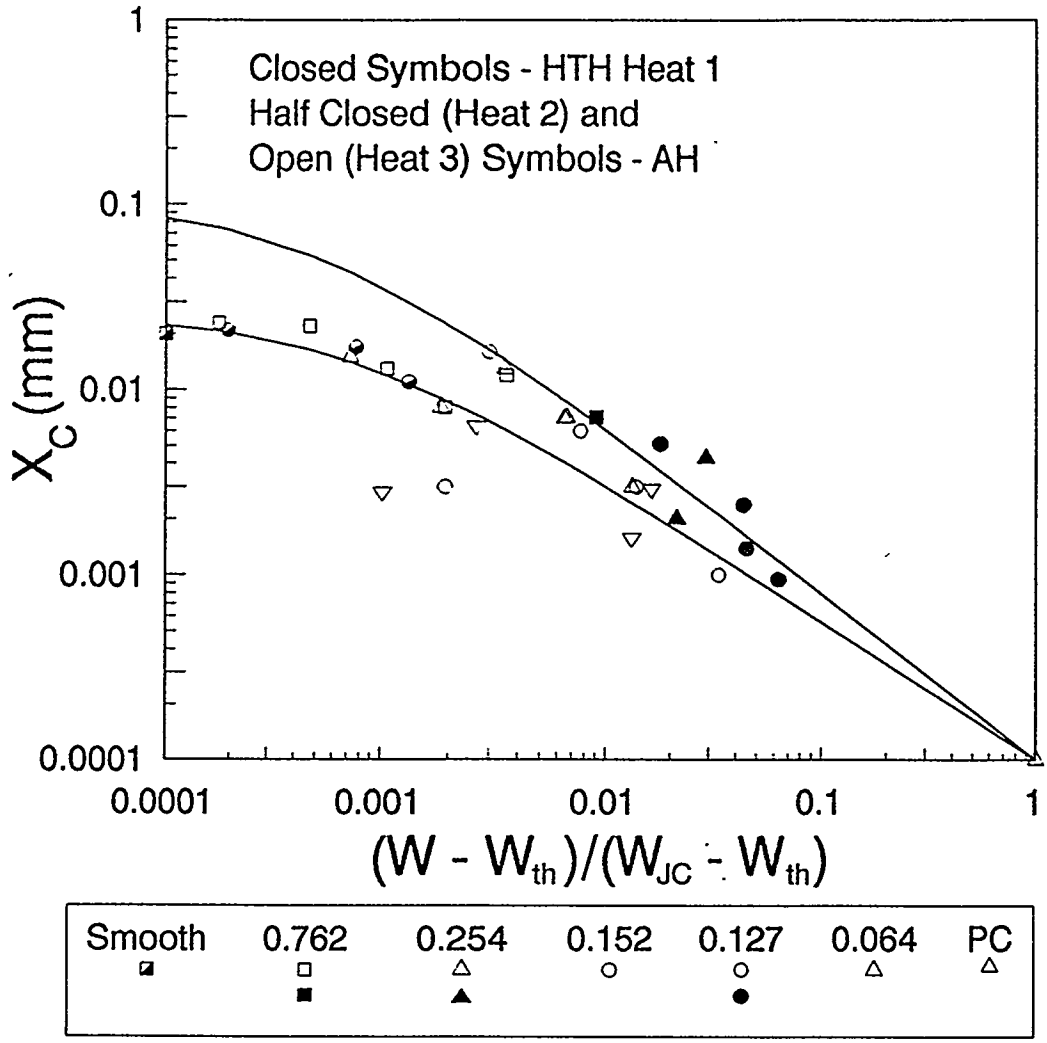

Fig. 4--The microstructurally characteristic distance for fracture initiation as a function the normalized applied strain energy density.

DISCUSSION

Mechanical Effects on SCC Initiation

A comparison of the HE and SCC fracture behaviors of AH and HTH heat treatments of Alloy X-750 provides insight relative to the micromechanics and mechanisms of environment-induced intergranular cracking in this alloy. Although these heat treatment conditions have very similar inert environment mechanical properties of yield strength and fracture toughness, the larger grained HTH condition has superior HE and SCC resistance. In the HE study, the notch fracture toughness of hydrogen charged HTH specimens was found to be superior to that of AH specimens in spite of its apparent lower critical SEDEN, W_c. The superior HE toughness of condition HTH was attributed to its much larger grain size. The larger microstructurally characteristic distance, X_c, results in a substantially lower applied

SEDEN at the grain boundary fracture initiation site, which more than compensates for the lower W_c (see Eq. 2.) The lower W_c for the HTH condition is consistent with the larger grain size as there is significantly less grain boundary area for distribution of embrittling elements known to lower the resistance of high nickel alloys to intergranular fracture [9,10].

The importance of mechanical effects on the initiation of SCC for Alloy X-750 is readily apparent in Fig. 4. There appears to be a mechanical threshold for initiation. For the AH heats, the threshold stress for smooth tensile specimens is about 4% higher than the proportional limit. Due to the superior SCC resistance of the HTH heat, there are no data near threshold to determine threshold stress for this heat treatment. The data trends for both heat treatments show that, for short exposure times, the apparent toughness extrapolates to the inert environment K_{JC} toughness of Alloy X-750. In between these limits of SCC and K_{JC} thresholds, the time dependent SCC initiation behavior is well behaved and can be correlated with equations of the form

$$t_i = t_o\left(\frac{W_e - W_{th}}{W_{JC} - W_{th}}\right)^{-m} = t_o\left(\frac{K_e - K_{th}}{K_{JC} - K_{th}}\right)^{-2m}, \qquad (10)$$

where, at 360°C in deaerated pure water, t_o = 3.3 h for both conditions AH and HTH, m = 0.7 for condition AH and m = 2.0 for condition HTH. This equation implies that the same mechanism for initiation of fracture applies over the entire stress range from the SCC threshold to stress intensities approaching K_{JC} fast fracture.

Environmentally Enhanced Creep Fracture Model

From Eq. 10, which describes the initiation behavior shown in Fig. 3, we conclude that the superior SCC initiation resistance of condition HTH can be attributed to whatever is responsible for the much stronger associated stress parameter dependence. One of the authors (MMH) recently developed an SCC crack growth rate model for Alloy X-750 and Alloy 600 that accounts for the stress intensity factor dependence of crack growth [11]. This model assumes that a hydrogen enhanced creep fracture mechanism controls the rate of crack advance. The model accounts for large effects of stress intensity factor and cold prestrain on the apparent activation energy. The model also accounts for the effects of these variables and temperature on the stress dependence of the crack growth rate.

Development of a similarly motivated model for SCC initiation is considered here. This model is based on the assumption of a transient creep constitutive equation that allows for creep hardening:

$$\dot{\varepsilon} = \frac{\dot{\sigma}}{E} + \frac{\dot{\sigma}}{NE}\left(\frac{\sigma}{\sigma_o}\right)^{\frac{1}{N}-1} + \dot{\varepsilon}_o\left(\frac{\sigma}{\sigma_o}\right)^{n}\left(\frac{\varepsilon}{\varepsilon_o}\right)^{-q}. \qquad (11)$$

In this equation N is the usual time-independent strain hardening exponent, q is the

creep strain hardening exponent, and n is the creep stress exponent. Reidel [12] has derived the crack tip stress distributions for materials that obey Eq. 11. He also provided an expression for the time dependence of the creep zone size:

$$r_{cz} = \alpha \frac{K^2}{E\sigma_o} (\dot{\varepsilon}_o t)^{\frac{1}{p}}, \tag{12}$$

where

$$p = \frac{Nn - 1 - q}{1 + N}, \tag{13}$$

and α is a function of N, n and q. Consistent with the time-independent model for HE cracking, we consider that SCC initiation occurs when the creep strain exceeds a critical value at a microstructurally characteristic distance from notch and crack tips. This requires that $r_{cz} > X_c$. Then the SCC initiation time is given by

$$t_i > \dot{\varepsilon}_o^{-1} \left(\frac{E \sigma_o x_c}{\alpha K^2} \right)^p. \tag{14}$$

In this equation $\dot{\varepsilon}_o$ is a temperature dependent material parameter, that, along with n and q, is expected to be environmentally sensitive.

Comparison of Eq. 14 with Eq. 10 implies that the stress parameter exponent in Eq. 10 can be obtained from Eq. 14. The strain hardening exponent, N, is about 0.167 for both AH and HTH conditions and the creep strain hardening exponent is typically 1 for low temperature-high stress dislocation creep [13]. We conclude then that it is the transient creep stress exponent, n, that distinguishes the AH and HTH conditions and is the deformation parameter associated with the superior SCC resistance of the HTH condition. Assuming these values for N, q and the values for p determined from Eq. 9, the creep stress exponents, n, are determined to be about 17 and 26 for AH and HTH conditions, respectively. There are no low temperature transient creep data for Alloy X-750 to give a comparison to these results. However, transient creep stress exponents this large indicate "exponential creep" [14], which is consistent with the expected low-temperature high-stress creep mechanism for SCC [11].

Effect of Source of Hydrogen on Crack Nucleation Site

An important difference to note between HE and SCC initiation for Alloy X-750 is in the sources of hydrogen. For the HE experiments, the hydrogen is internal to the specimen and crack nucleation occurs at a grain boundary located at a distance of one grain diameter from the notch and crack tips. This initiation site is independent of notch radius, applied stress intensity factor and the precharged internal hydrogen concentration. For SCC crack initiation, which is also intergranular, the source of

hydrogen is external to the specimen. In this case the crack initiation site varies systematically from about 0.1 μm to one grain diameter from the notch tip, according to the analysis above.

These effects can be rationalized in terms of the hydrogen and strain gradients. For the HE case, the specimens are first precharged with a uniform distribution of hydrogen and then strained to initiation. In this case of uniform hydrogen, a microcrack should first nucleate at a distance of one grain diameter if the crack nucleation occurs by a Stroh [15]-Cottrell [16]-Petch [17]-type crack nucleation mechanism. In this mechanism cracks nucleate at the terminus of a dislocation pile-up. The strength of the pile-up is proportional to $\sqrt{l}$, where l is the length of the pile-up. Then microcracks will first nucleate at a distance of one grain diameter from a source of dislocations, such as a notch, since the maximum length of a dislocation pile-up is one grain diameter.

For the SCC case, specimens are first strained and then exposed to a source of hydrogen by exposure to high temperature deaerated water. A uniform hydrogen distribution is not expected for sharply notched specimens. Hydrogen may enter at a notch tip preferentially due to localized creep disruption of the corrosion oxide. Moreover, hydrogen will be trapped in the strain field of the notch in proportion to the local strain level [18,19]. The notch strain at the characteristic distance is a function of the ratio $K/\sqrt{\rho}$, which is a measure of the maximum local strain and magnitude of the strain gradient [20,21]. As this ratio increases, either by an increase in K or a decrease in ρ, the maximum strain and the strain gradient increase, and consequently, so will also the hydrogen concentration and hydrogen gradient. Then crack nucleation should occur near the notch tip where the strength of a dislocation pile-up first exceeds the local hydrogen affected fracture strength. In the limit of large $K/\sqrt{\rho}$, which is approached with a sharp crack, the crack nucleation site approaches very near the surface for the external hydrogen case.

For very blunt notches the strain distributions, and consequently, the hydrogen distributions, will be more uniform. In the limit of the unnotched tensile specimen, the hydrogen distribution is uniform and the specimen is expected to behave in a way similar to the internal hydrogen case. Therefore, as the notch radius increases we expect that the crack initiation will occur at a site that approaches one grain diameter from the notch tip.

CONCLUSIONS

Use of the strain energy density-distance criterion, which was developed for rising-load K_c initiation of cracking due to hydrogen embrittlement, shows that stress corrosion cracking, like HE cracking, also initiates at an interior site. This supports an assumption that hydrogen plays an important role in SCC initiation as the water environment has no access to the initiation site. Since initiation occurs under static load, time-dependent creep strain appears to be necessary. Since the threshold stress for crack initiation is just above the proportional limit, dislocation mechanisms, such as thermally activated glide, are most likely. Consideration of the analytical solutions available for crack tip deformation under creep conditions suggest that the SCC stress dependence is a function of the time-independent and creep hardening exponents but is

likely controlled by the transient creep stress exponent.

Unlike HE, the site for SCC initiation depends on the notch radius and the applied stress intensity factor. The existence of hydrogen gradients, which are due to strain-induced trapping of hydrogen at notch and cracks tips, can qualitatively account for variation in the site for microcrack nucleation. These observations and conclusions are seen to be consistent with the observations from a previous HE study in which the characteristic distance for microcrack nucleation was found to be independent of notch radius, applied stress intensity factor and hydrogen level.

ACKNOWLEDGMENTS

The authors wish to acknowledge H. K. Shen and J. J. Kearns whose data were used in this study. This work was supported by the United States Department of Energy through Contract No. DE-AC11-93PN38195.

REFERENCES

[1] Berge, P., "Experience with Alloy X-750 in PWRs," Proceedings: 1986 Workshop on Advanced High Strength Materials, EPRI NP-6363, 1989.

[2] Carnahan, R. A. and Gordon, G. M., "Summary of Alloy X-750 Behavior in General Electric BWRs," Proceedings: 1986 Workshop on Advanced High Strength Materials, EPRI NP-6363, 1989.

[3] Benhamou, C. and Poitrenaud, P., "Framatome Experience and Programs in Relation to Guide Tube Support Pin Cracking," Proceedings: 1986 Workshop on Advanced High Strength Materials, EPRI NP-6363, 1989.

[4] Hirose, Y. and Mura, T., "Nucleation Mechanism of Stress Corrosion Cracking from Notches," Engineering Fracture Mechanics, Vol. 19, No.2, 1984, pp. 317-329.

[5] Hall, M. M., Jr., Symons, D. M. and Kearns, J. J., "Strain Energy Density - Distance Criterion for the Initiation of Hydrogen - Induced Cracking of Alloy X-750," Proceedings of the Parkins Symposium on Fundamental Aspects of Stress Corrosion Cracking, S. M. Bruemmer, E. I. Meletis, R. H. Jones, W. W. Gerberich, F. P. Ford, and R. W. Staehle, Ed., The Minerals, Metals and Materials Society, 1992, pp. 231-244.

[6] Mills, W. J. et al., "Effect of Irradiation on the Stress Corrosion Cracking Behavior of Alloy X-750 and Alloy 625," Sixth International Symposium on Environmental Degradation of Materials in Nuclear Power Systems - Water Reactors, R. E. Gold and E. P. Simonen, Ed., 1993, pp. 633-643.

[7] Saxena, A. and Hudak, S. J., "Review and Extension of Compliance Information for Common Crack growth Specimens," International Journal of

Fracture, Vol. 14, No. 5, 1978, pp. 453-468.

[8] Symons, D. M. and Thompson, A. W., "The Effect of Hydrogen on the Fracture of Alloy X-750," Metallurgical and Materials Transactions A, Vol. 27A, January 1996, pp. 101-110.

[9] Grove, C. A. and Petzold, L. D., Corrosion of Nickel-Base Alloys, American Society for Metals, 1985, pp. 165-180.

[10] Elliott, C. K., "Effect of Thermal Treatment on the Fracture Properties of Alloy X-750 in Aqeous Environments," Ph. D. Thesis, Massachusetts Institute of Technology, 1985.

[11] Hall, M. M. Jr., "Thermally Activated Dislocation Creep Model for Primary Water Stress Corrosion Cracking of NiCrFe Alloys," Presented at the International Symposium on Plant Aging and Life Prediction of Corrodible Structures, Japan Society of Corrosion Engineering, Sapporo, Japan, 1995, WAPD-T-3045.

[12] H. Riedel, Creep Deformation at Crack Tips in Elastic-Viscoplastic Solids," Journal of the Mechanics and Physics of Solids, Vol. 29, 1981, 35-49.

[13] Feltham, P., "Creep and Stress Relaxation in Alpha-Brass at Low Temperatures," Philosophical Magazine, Vol. 6, 1961, pp. 259-270.

[14] Sherby, O. D. and Burke, P. M., Mechanical Behavior of Crystalline Solids at Elevated Temperature, Pergamon Press Ltd., London, 1968, p. 340.

[15] Stroh, A. N., Proceedings of the Royal Society, Vol. A223, 1954, p. 404-414.

[16] Cottrell, A. H., Transactions of the American Institute of Mining, Metallurgy and Petroleum Engineers, Vol. 212, 1958, pp. 192-203.

[17] Petch, N. J., Philosophical Magazine, Vol. 3, 1958, p. 1089.

[18] Bursar, J. M., de Beaver, O., Gras, J. M., Noel, D., Ribs, R. and Valent, F., "SCC of Alloy 600 in High Temperature Water: A Study of Mechanisms," Corrosion-Deformation Interactions CD 92, Las Editions de Physics, Las Ails, France, 1992, pp. 117-137.

[19] Agnosia, T., Yamaguchi, Y. and Iijima, Y., "Electron Micro Autoradiographic Observation of Tritium Distribution on Alloy X750," Sixth International Symposium on Environmental Degradation of Materials in Nuclear Power Systems - Water Reactors, R. E. Gold and E. P. Simonen, Ed., 1993, pp. 799-804.

[20] Rice, J. R., "A Path Independent Integral and the Approximate Analysis of Strain Concentration by Notches and Cracks," Journal of Applied Mechanics, Vol. 35, June 1968, pp. 379-386.

[21] Santhanam, A. T. and Bates, R. C., "The Influence of Notch-tip Geometry on the Distribution of Stress and Strain," Materials Science and Engineering, Vol. 41, 1979, pp. 243-250.